Supporting Information

Multifunctional Polyzwitterion Ionic Liquid Coating for Long-Lifespan and Dendrite-Free Zn Metal Anodes

Yanqun Lv, [ab] *Ying Xiao,* [b] *Shuting Xu,* [c] *Feng Huo,* [c] *Yong Chen,*[b] *Ming Zhao,* [b] *Lili Liu,* [d] Chang Su, [a]* *Yanli Zhu,* [e*] *and Shimou Chen* [b]*

[a] *College of Chemical Engineering, Shenyang University of Chemical Technology, Shenyang, 110142, China.*

[b] *State Key Laboratory of Chemical Resource Engineering, Beijing Key Laboratory of Electrochemical Process and Technology of Materials, Beijing University of Chemical Technology, Beijing, 10029, China.*

[c] *Institute of Process Engineering, Chinese Academy of Sciences, Beijing, 100190, China.*

[d] *College of Chemistry and Materials Engineering, Beijing Technology and Business University, Beijing, 100048, China.*

[e] *State Key Laboratory of Explosion Science and Technology, Beijing Institute of Technology, Beijing, 100081, China.*

**Corresponding Authors* E-mail:

suchang@syuct.edu.cn, zhuyanli1999@bit.edu.cn, chensm@mail.buct.edu.cn,

The preparation of P(SBMA-*co*-BuA)-5: 1 mmol SBMA, 19 mmol *tert*-BuA and 0.03 g AIBN were dissolved in 30 mL isopropanol in an oil bath at 60 ℃ for 3 h. Then MEHQ was added to terminate the reaction. Subsequently, the polymerization was precipitated in DI water and washed three times with DI water. Finally, the sample was dried under vacuum at 70 ℃ for 12h. Poly(SBMA-*co*-*tert*-BuA)-3 and poly(SBMA-*co*-*tert*-BuA)-7 and Poly(SBMA-*co*-*tert*-BuA)-10 with the content of 3 mol%, 7 mol% and 10 mol% SBMA were prepared in the same way, and poly(*tert*-BuA) was obtained without addition of SBMA.

The preparation of Zn@P(SBMA-*co*-BuA): 2 g PVDF (Mw = 1 000 000) was dissolved in 50 mL DMF under magnetic stirring to form a slightly viscous transparent solution. Then, 2.5 g P(SBMA-*co*-BuA) was added to the above solution. After being stirred for 12 h, a homogeneous slurry was obtained. The obtained slurry then cast onto Zn foil by common doctor blading method. The as-prepared Zn@P(SBMA-*co*-BuA) was transferred into vacuum oven to remove the solvent prior to use at 80 ℃. For the preparation of Cu@P(SBMA-*co*-BuA), the process was the same as the above steps, but the zinc foil was replaced with copper foil.

The preparation of MnO_2: MnO_2 powders were prepared according to the previous work[22]. 1 mL of 0.5 M H_2SO_4 solution was added into 45 mL of 0.003 M $MnSO_4$ solution under magnetically stirring until a transport solution. Subsequently, 10 ml 0.1 M $KMnO_4$ aqueous solution was added into the above solution drop by drop. After stirring the mixed solution for 2 h, transfer above mixture to a 100 mL Teflon-lined autoclave, and heat it at 120 ℃ for 12 h. Then, the powders were rinsed with DI water

and dried at 80 ℃ overnight.

The preparation of $Mg_{0.1}V_2O_5·H_2O$: $Mg_{0.1}V_2O_5·H_2O$ powders were prepared according to the previous work[54]. 1.2867 g magnesium acetate was added into 120 mL of 1.404 g ammonium metavanadate water solution with continuous magnetic stirring at 80 °C until form a transport solution, and 30 mL of acetic acid were added to the above solution drop by drop. Then the above solution was transferred to three 100 mL Teflon-lined autoclaves and maintained at 180 °C for 48 h. Finally, the obtained dark green product was thoroughly washed with deionized water and dried at 80 °C for 12 h.

The preparation of N-doped porous carbon (NC): the **NC** was prepared from the carbonization of ZIF-8[53]. Zinc acetate (8.61 g) and 2-methylimidazole (30 g) were dissolved into 200 ml deionized water respectively (solution A and B). The two solutions were then mixed together at room temperature to generate ZIF-8 after two days of aging, which was further washed by deionized water and vacuum dried. Finally, successive operations of calcination at 900 ℃ under N_2 atmosphere were carried out to generate NC.

Preparation of electrolyte for pouch cells: 1 g AM monomer was dissolved in 5 mL 2 M $ZnSO_4$ solution under magnetic stirring to form a transparent solution. Then 0.3 mL of N, N′-methylene-bis(acrylamide) (10 mg mL^{-1}) and 0.4 mL of ammonium persulfate (5 mg mL^{-1}) were added into the above solution and stirred for 10 min. The as-prepared mixture solution was introduced in a glass plate mold (thickness = 1 mm) followed by UV irradiation (35W, 365 nm, Zhonglian) for 2 h, obtaining the PAM hydrogels electrolytes.

Characterizations: The crystallographic data of samples were obtained by a Bruker D2

Phaser X-Ray Diffractometer with Cu Kα radiation (λ = 1.5406 Å) at a voltage of 30 kV and a current of 10 mA. The morphologies of samples were characterized by scanning electron microscopy (SEM; TESCAN, MAIA3 XMU). The Fourier transform infrared spectroscopy (FTIR) mapping was performed with NEXUS 670 FT-IR Instrument. Atomic force microscopy (AFM) images were acquired in tapping mode on a Dimension (Bruker). The contact angles were measured on the SL250 Contact Angle Measuring System (KINO, America).

Electrochemical Test: The electrochemical performances of the CR2025 coin-type cells or pouch cells assembled in this work were studied on a Land BT2000 battery test system. Zinc foil was sanded with fine sandpaper (3000 mesh, 7000 mesh and 10000 mesh) and rinsed with DI water and ethanol before using. Glass microfiber filters (Whatman) membrane as the separator (Φ 16 mm) and 2 M $ZnSO_4$ solution was used as the electrolyte. For coin cells, Zn foil, and Cu foil were cut into disk-shaped electrodes with a diameter of 12 mm. The stability of Zn anode was tested by Zn//Zn and Zn@P(SBMA-*co*-BuA)//Zn@P(SBMA-*co*-BuA) cell. The Coulombic efficiency of Zn plating/stripping was using Zn//Cu and Zn//Cu@P(SBMA-*co*-BuA) cells. For the cathodes, The $Mg_{0.1}V_2O_5{\cdot}H_2O$, MnO_2, and NC cathode material were prepared by compressing active material, Ketjen Black and polytetrafluoroethylene preparation (60 wt%) at a weight ratio of 7:2:1. For Zn//$Mg_{0.1}V_2O_5{\cdot}H_2O$ or Zn//MnO_2 coin cells, aqueous electrolyte (2 M $ZnSO_4$ or 2 M $ZnSO_4$ + 0.1 M $MnSO_4{\cdot}H_2O$) and PAM were used as the electrolyte.

The cyclic voltammetry (CV) measurement recorded with Autolab workstation

(PGSTAT302N) with a scan speed of 0.1 mV/s. The electrochemical impedance spectra (EIS) of the coin cells were also executed on the Autolab workstation, the frequency range from 1MHz to 1 Hz. Linear polarization measurements were conducted in a three-electrode system with bare Zn and Zn@P(SBMA-*co*-BuA) as the working electrode, Pt plate as the counter electrode, and Ag/AgCl as the reference electrode. The corrosion potential and corrosion current were calculated from Tafel fit system in electrochemical workstation. HER tests were conducted in a three-electrode system with bare Zn and Zn@P(SBMA-*co*-BuA) as the working electrode, Pt plate as the counter electrode, and Ag/AgCl as the reference electrode in a 2 M Na_2SO_4 electrolyte (conducted using Autolab). The LSV measurement was carried out at a scan rate of 5 mV s^{-1}. Exchange current densities were measured through fitting Tafel plots for Zn//Zn symmetric coin cells at a scan rate of 5 mV s^{-1} in a voltage range of -0.1 to 0.1 V[44]. Moreover, the Zn@P(SBMA-*co*-BuA) and bare Zn electrodes were also assembled into transparent symmetric cells, followed by an in situ optical observation to detect electrode evolution during Zn plating/stripping process at a current density of 10 mA cm^{-2}.

Density functional theory (DFT) calculations: Firstly, the structures of SBMA, SO_4^{2-}, H_2O, Zn^{2+} and their complexes (SBMA with SO_4^{2-}, H_2O, Zn^{2+}, and SBMA) were optimized by using DFT at the b3lyp/6-311+g(d, p) level[62]. All geometry optimizations including the implicit solvent effect with SMD were performed using the Gaussian 09 package. Then, to better describe the electrostatic-dominated weak interactions, DFT-D3[63] dispersion correction was introduced on top of the previous basis set, and the single-point energies of the four complexes were calculated, and the

DFT-D3 correction energy was first added to the nuclear repulsion, the final output total energy is the DFT-D3 corrected energy, $E_A=E_{A\text{-origin}}+E_{disp}^{DFT-D3}$. The interaction energy of the four complexes can be expressed by formula: $E_{inter}=E_{AB}-(E_A+E_B)$. Where E_A and E_B respectively represent the energies of A (SBMA, SO_4^{2-}, H_2O, Zn^{2+}) and B (SBMA). The E_{inter} is a negative value, the more negative the energy, the more stable the structure.

$$E_{disp}^{DFT-D3}=-\frac{1}{2}\sum_{A\neq B}\sum_{n=6,8}s_n\frac{C_n^{AB}}{R_{AB}^{\ n}+f(R_{AB}^{\ 0})^n}$$

Self-Diffusion Coefficient: All the simulations in this work are completed using the large-scale atomic/molecular massively parallel simulator (LAMMPS)[64]. The parameters of bond, angle, dihedral, van der Waals interactions and electrostatic interactions are described by the GAFF force field[65-66], while the electrostatic interactions are optimized when fitting electrostatic potentials. The timestep for integrating Newtonian equations of motion is 2 fs. All the simulations were equilibrated in the NPT ensemble for at least 30 ns with the constant temperature (298.15K) and the pressure of 1.0 atm.

The mean square displacements (MSD) calculated from equation:

$$\langle[r(t)-r(0)]^2\rangle=\frac{1}{n+1}\sum_{t_0=0}^{n}\frac{1}{N}\sum_{i=1}^{N}\left[r_i(t_0+t)-r_i(t_0)\right]^2$$

Where the t_0 are the different time origins, and N is the number of molecules and $r_i(t)$ is the position of molecule i at time t. The self- diffusion coefficient is computed using the following Einstein expression：

$$D_S=\frac{1}{6}\lim_{t\to\infty}\frac{d}{dt}\langle[r(t)-r(0)]^2\rangle$$

Where the slope is fit over the linear region of MSD.

Potential of mean force (PMF): A polymer-electrolyte solution interface model was equilibrated in the NPT ensemble for at least 10 ns. A series of umbrella sampling was carried out to obtain the free energy profile along the transport path of Zn^{2+} and H_2O inserting into the polymer layer. By using several options of steered MD (SMD), which allows to induce conformational changes in systems and to compute the potential of mean force (PMF) along the assumed reaction coordinate. Comparing the energy barriers of Zn^{2+} and H_2O into the polymer layer, demonstrating the hydrophobic nature of the polymer.

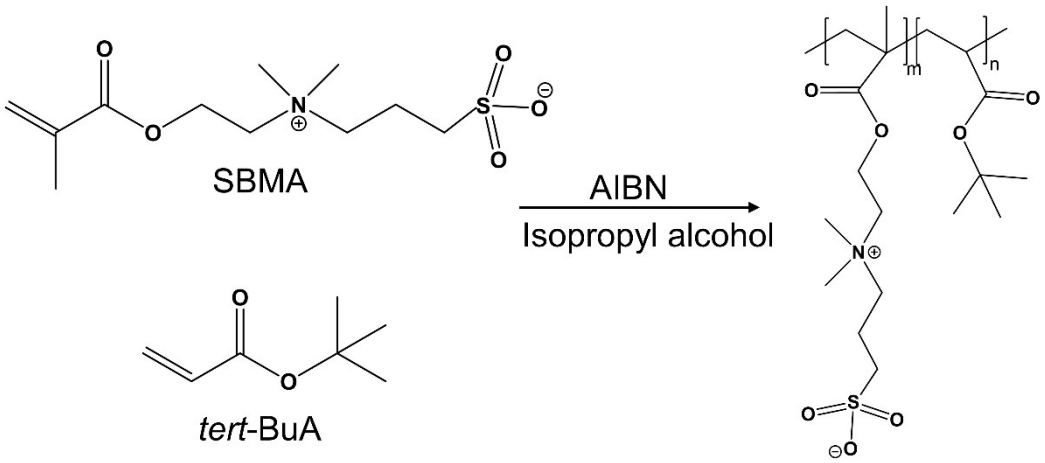

Figure S1. Synthesis of P(SBMA-*co*-BuA)

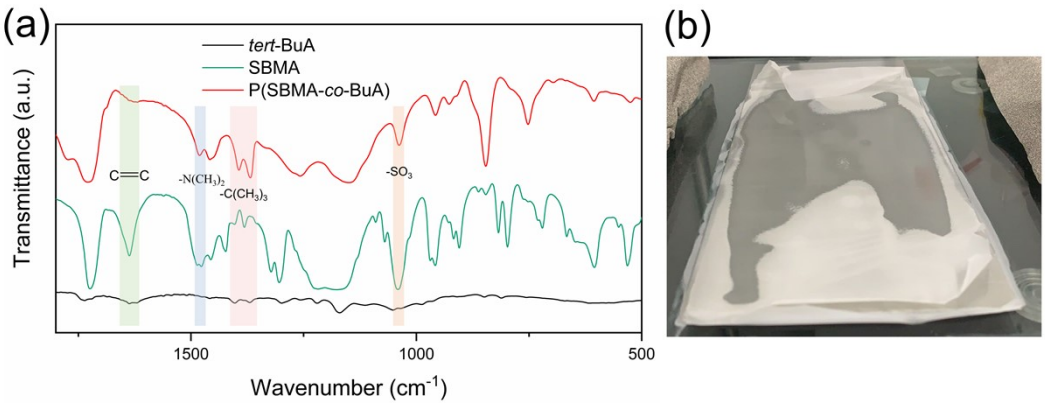

Figure S2. a) The FTIR spectra of *tert*-BuA, SBMA and P(SBMA-*co*-BuA). b) the optical image of in situ polymerized P(SBMA-*co*-BuA) coating.

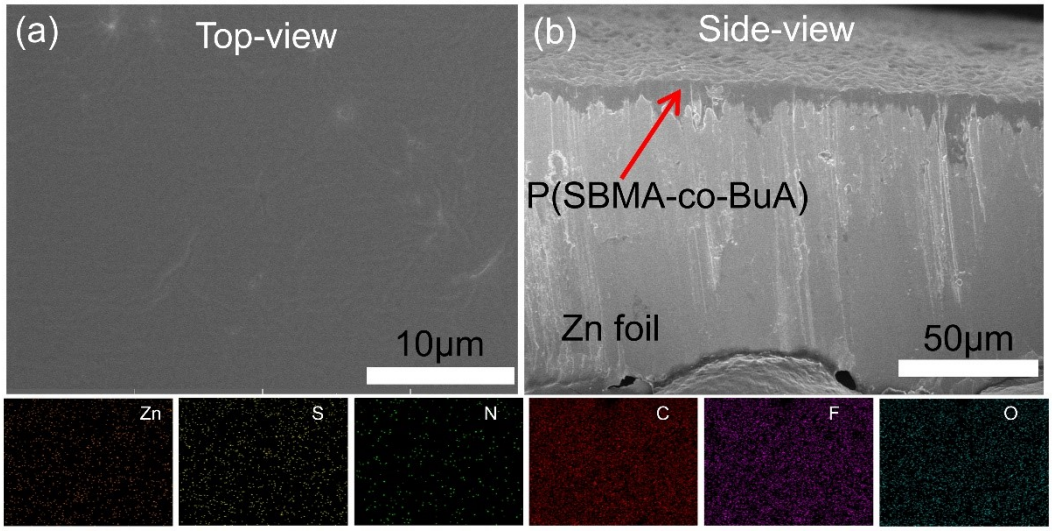

Figure S3. The a) top-view and b) side-view SEM image and elemental mappings of the Zn@P(SBMA-*co*-BuA).

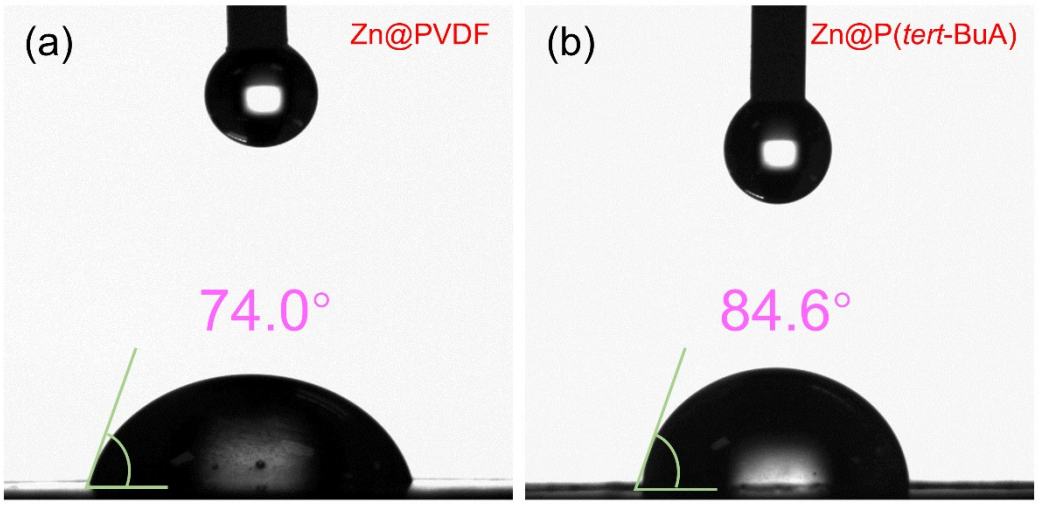

Figure S4. The contact angles of the Zn@PVDF and Zn@P(*tert*-BuA) anodes.

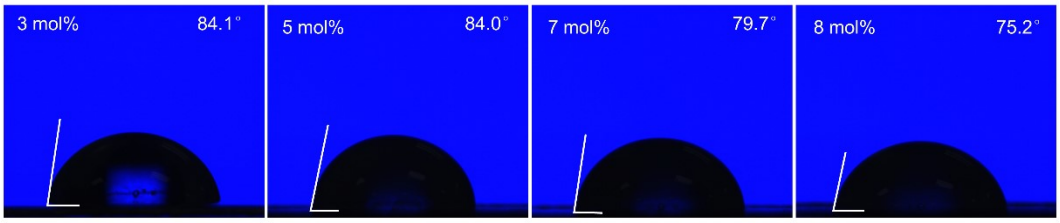

Figure S5. The contact angle of the coated Zn with the different concentration of the SBMA.

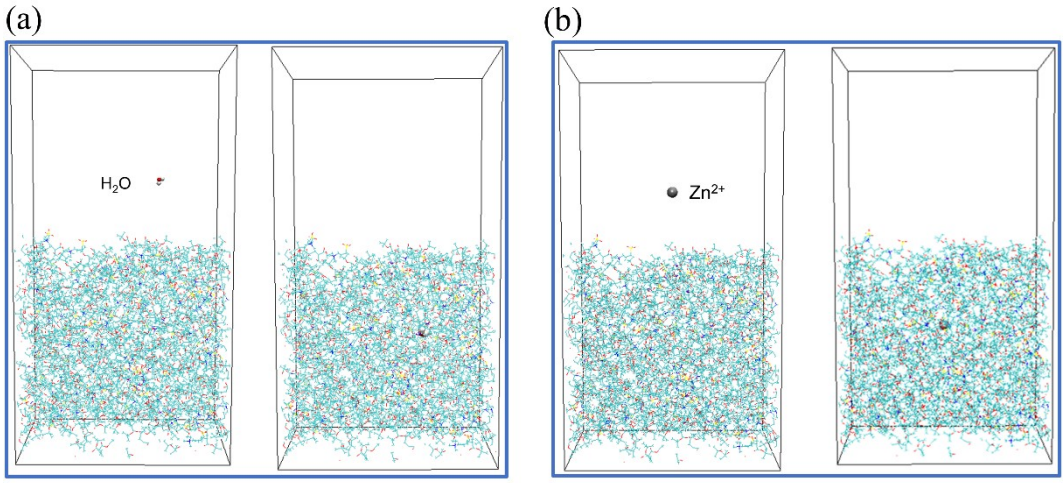

Figure S6. a) Molecular dynamics simulated structure of the H_2O molecule in the inserting process. b) Molecular dynamics simulated structure of the Zn^{2+} in the inserting process.

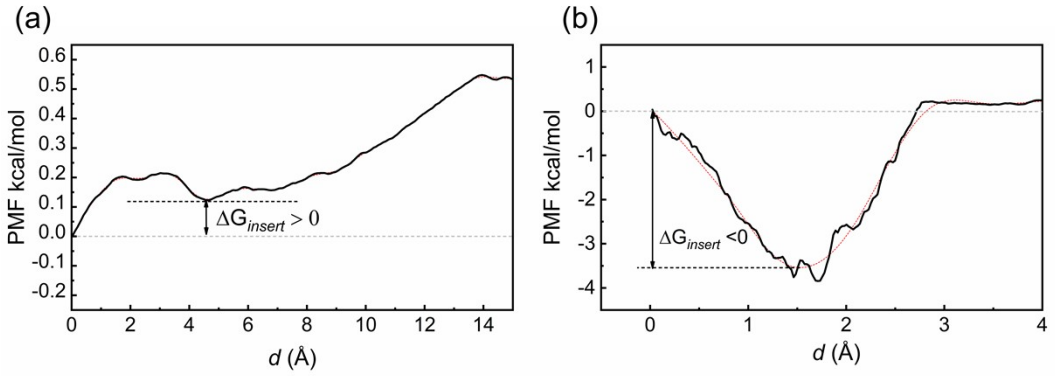

Figure S7. (a) PMF for the water molecule inserting into the P(SBMA-*co*-BuA). (b) PMF for the Zn^{2+} inserting into the P(SBMA-*co*-BuA).

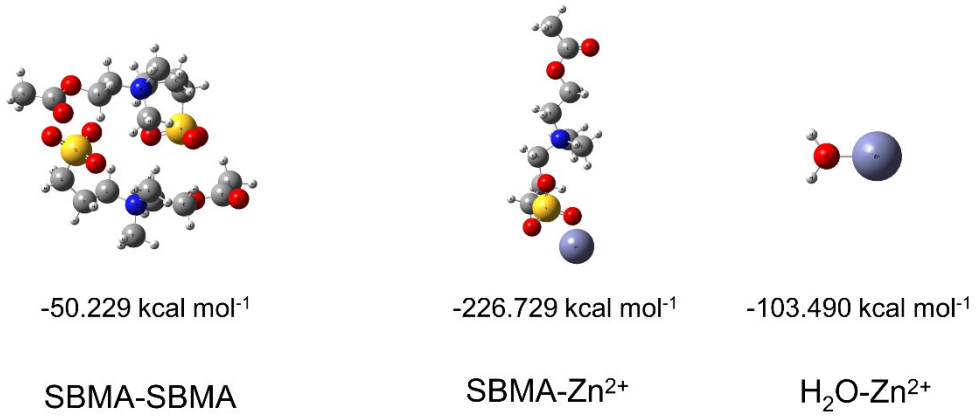

Figure S8. DFT calculation of the interaction between different components in SBMA-SBMA, SBMA-Zn^{2+}, and H_2O-Zn^{2+}.

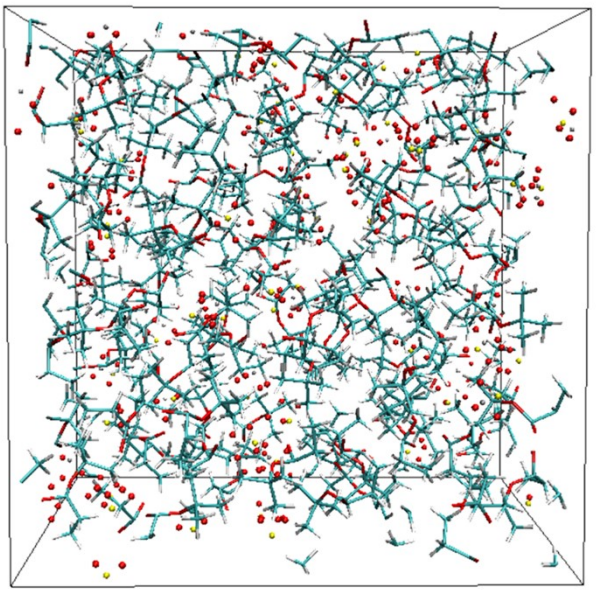

Figure S9. Molecular dynamics simulated structure of the Zn-*tert*-BuA model.

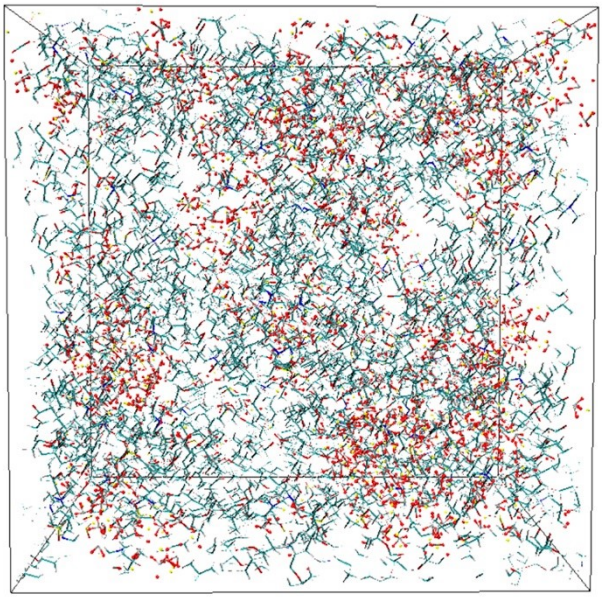

Figure S10. Molecular dynamics simulated structure of the Zn-SBMA-*co*-BuA model.

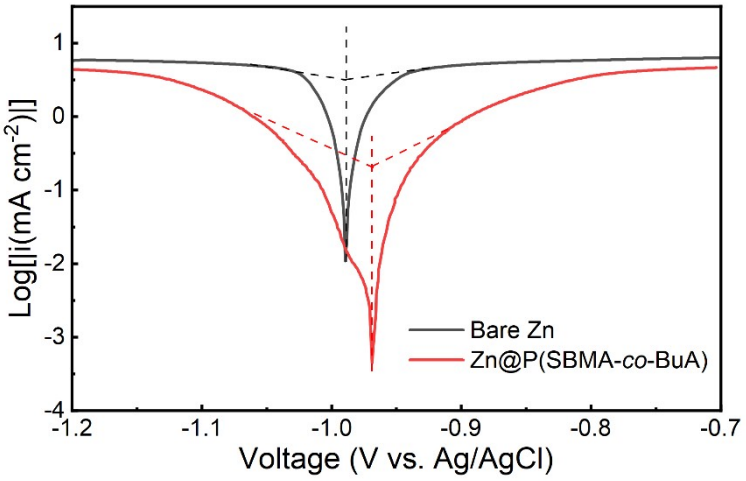

Figure S11. Linear polarization curves for describing corrosion of different Zn anodes.

Table S1: Corrosion potential and corrosion current density of bare Zn and Zn@P(SBMA-*co*-BuA).

Electrode	E_{corr} (V)	J_{corr} (mA cm^{-2})	I (%)
Bare Zn	-0.98916	3.1623	-
Zn@P(SBMA-*co*-BuA)	-0.96855	0.2042	93.54

The inhibition efficiency (I) was used to evaluate the protective effect of the P(SBMA-*co*-BuA) coating on the Zn anode, which be calculated according the following equation[1]:

$$I = (J_{corr} - J'_{corr})/J_{corr}$$

where J_{corr} and J'_{corr} are the corrosion current density of bare Zn and Zn@P(SBMA-*co*-BuA), respectively.

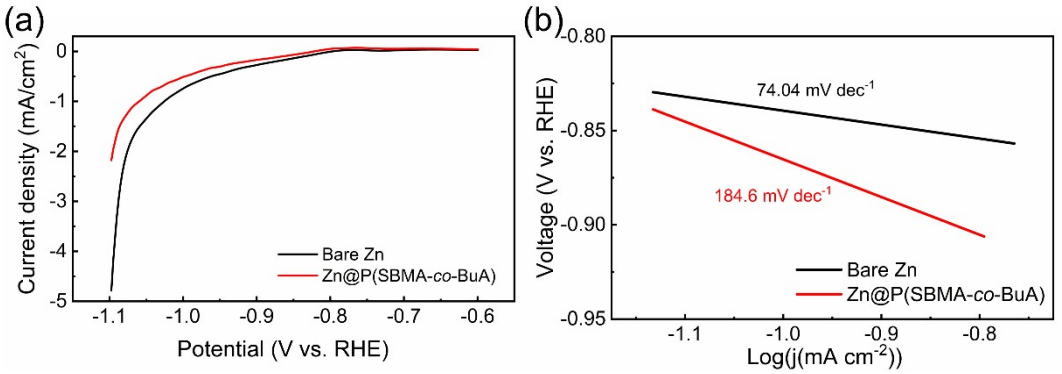

Figure S12. a) Hydrogen evolution polarization curves of bare Zn and Zn@P(SBMA-*co*-BuA) electrode in 2 M Na_2SO_4 solution. b) Tafel plots for calculating Tafel slopes.

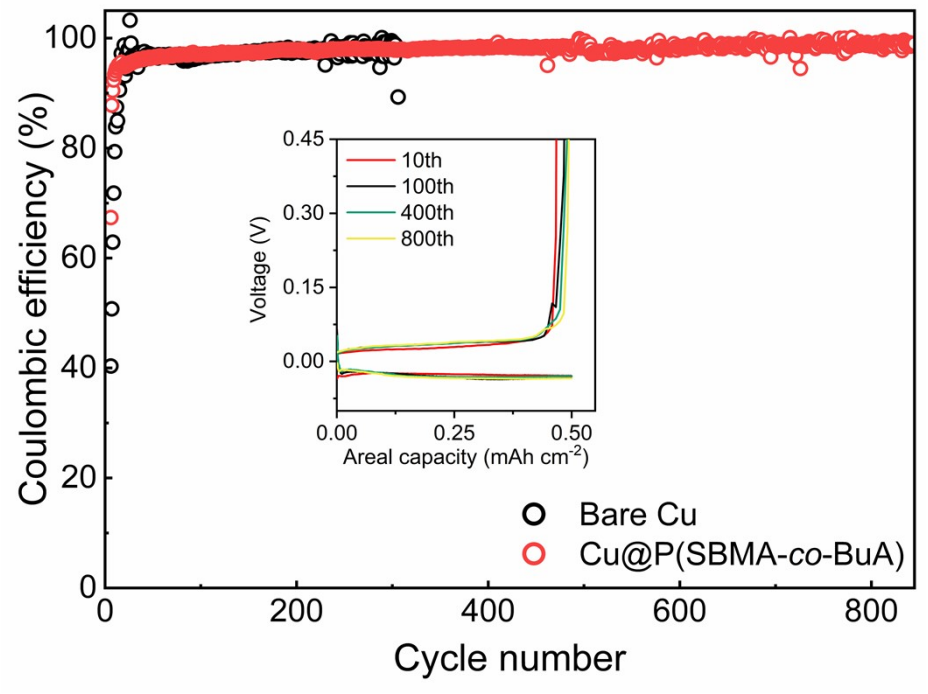

Figure S13. Coulombic efficiencies of Zn plating/stripping process in Zn@P(SBMA-*co*-BuA)//Cu and bare Zn//Cu cells at 0.5 mA cm^{-2} with a capacity of 0.5 mAh cm^{-2}. Inset: Corresponding voltage profiles at the various cycle.

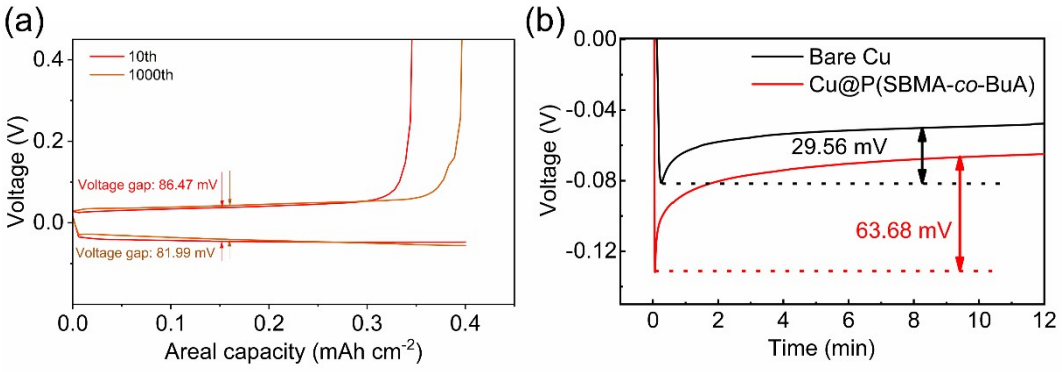

Figure S14. a) Charge-discharge voltage profiles of Zn//P(SBMA-*co*-BuA)@Cu cell at the 10th and 1000th cycles. b) Nucleation overpotential for bare Zn and Zn@P(SBMA-*co*-BuA) symmetric cells at the current densities and areal capacities of 2.0 mA cm^{-2} and 0.4 mAh cm^{-2}.

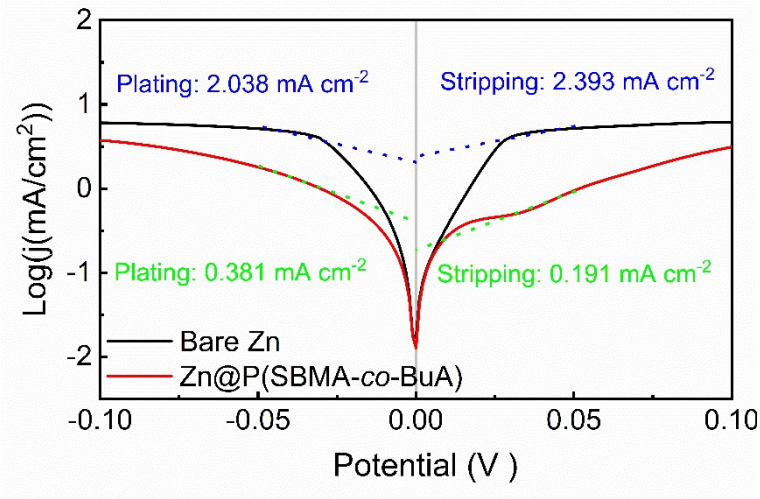

Figure S15. Tafel curves of symmetric cells with bare Zn and Zn@P(SBMA-*co*-BuA) electrodes.

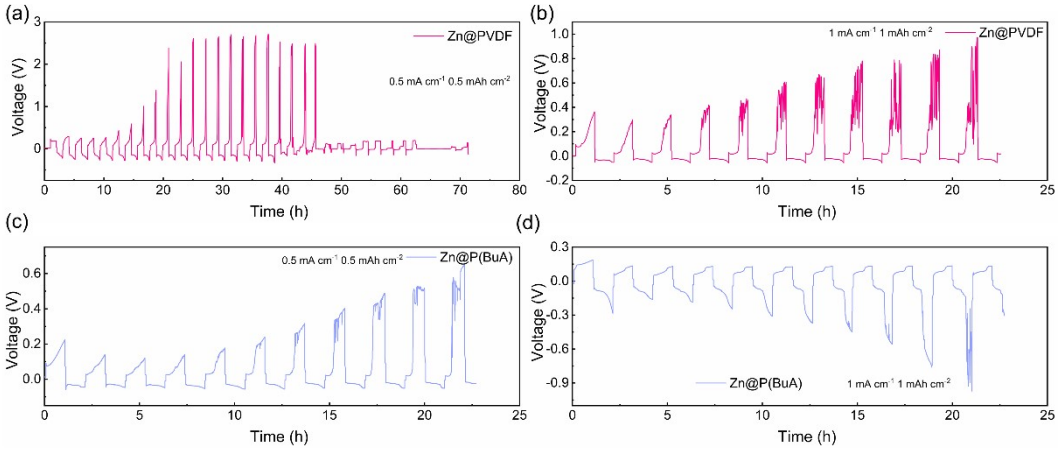

Figure S16. a-d) Cycling performance of symmetrical cells with Zn@PVDF and Zn@P(*tert*-BuA) electrode at different current density of 0.5 mA cm^{-2} and 1mA cm^{-2}.

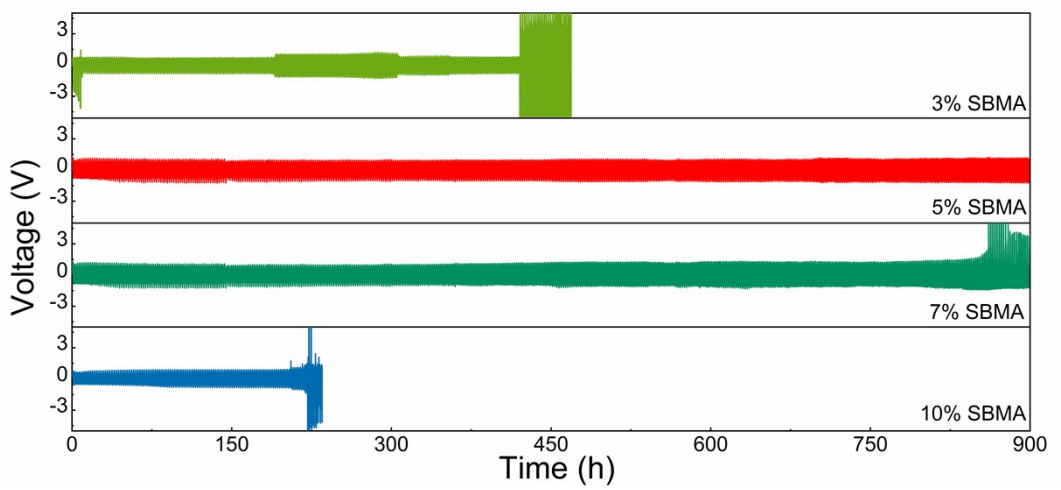

Figure S17. Zn//Zn symmetrical cells with different SBMA at 1 mA cm^{-2} and 1 mAh cm^{-2}

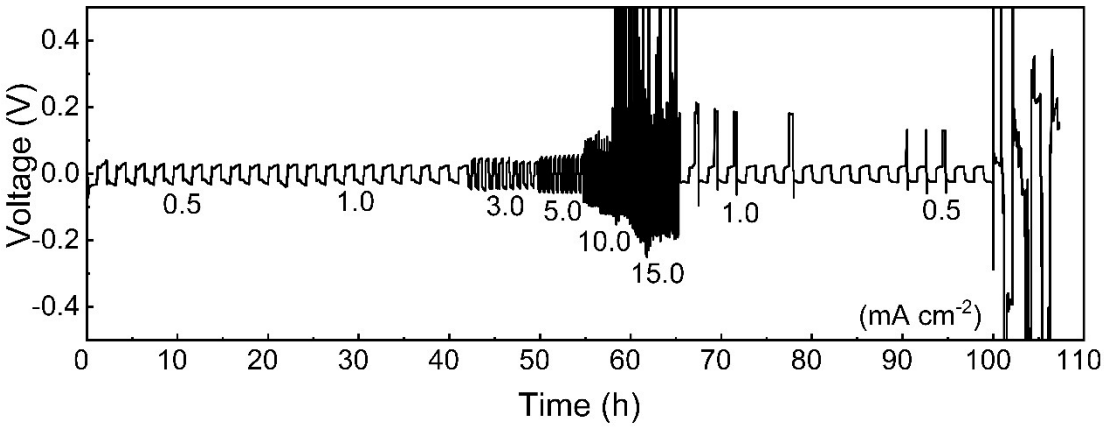

Figure S18. Rate performance of symmetrical cells using bare Zn.

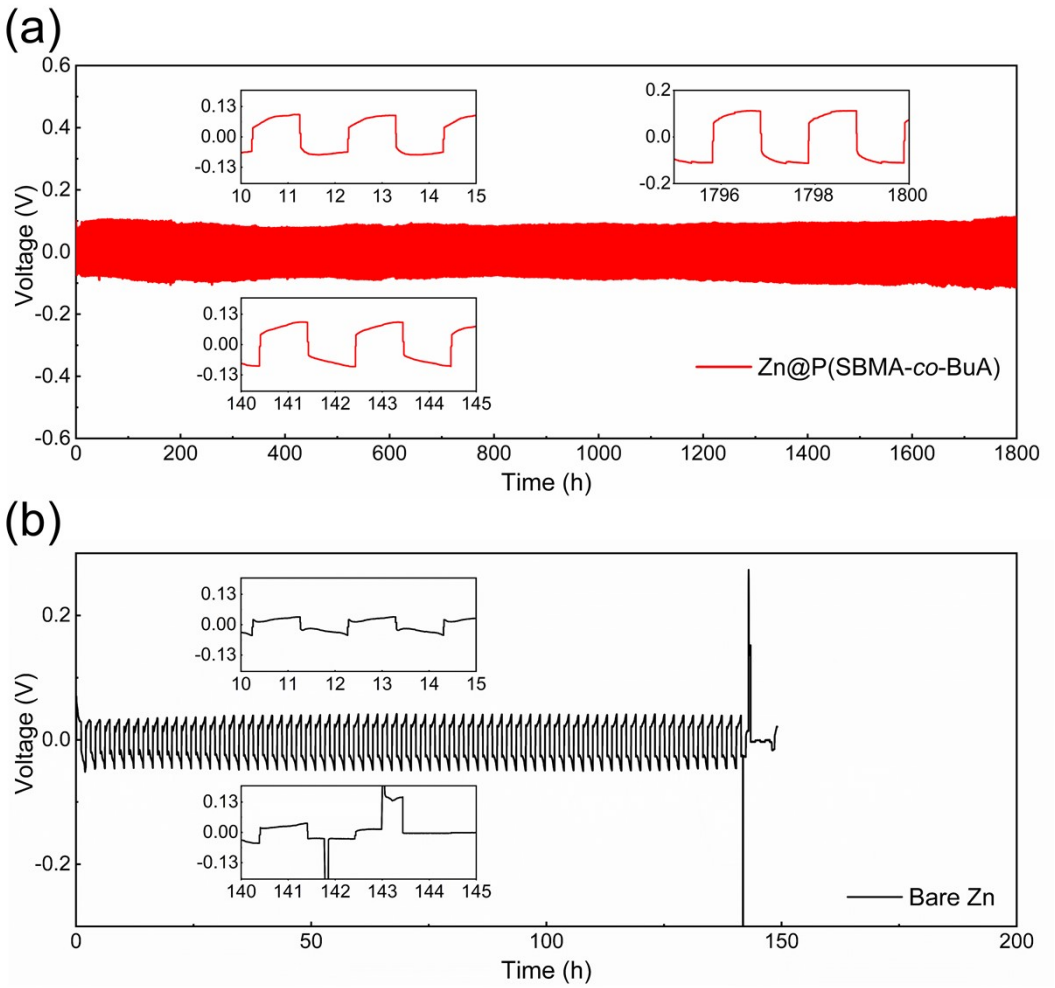

Figure S19. a) Zn//Zn symmetrical cells with Zn@P(SBMA-*co*-BuA) and b) bare Zn at 0.5 mA cm^{-2} and 0.5 mAh cm^{-2}.

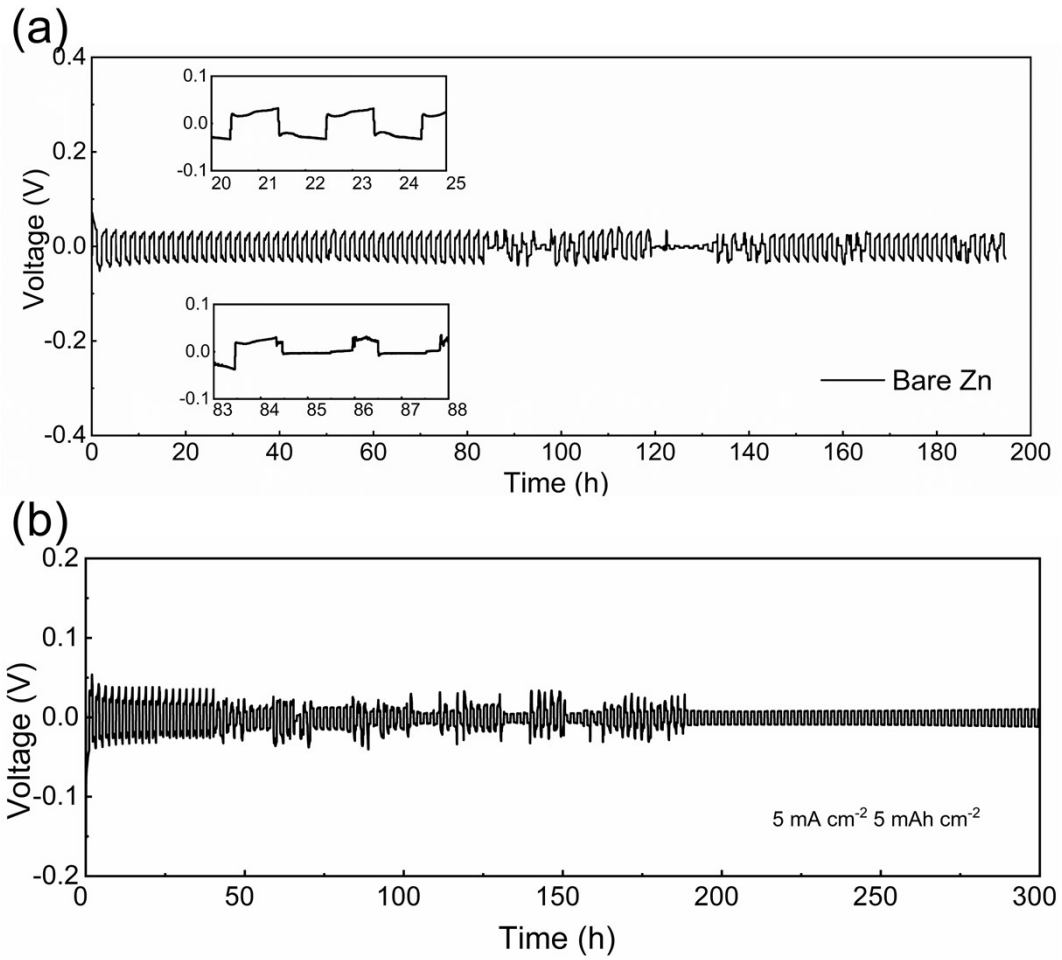

Figure S20. Zn//Zn symmetrical cells with bare Zn at a) 1 mA cm^{-2} and 1 mAh cm^{-2} and b) 5 mA cm^{-2} and 5 mAh cm^{-2}.

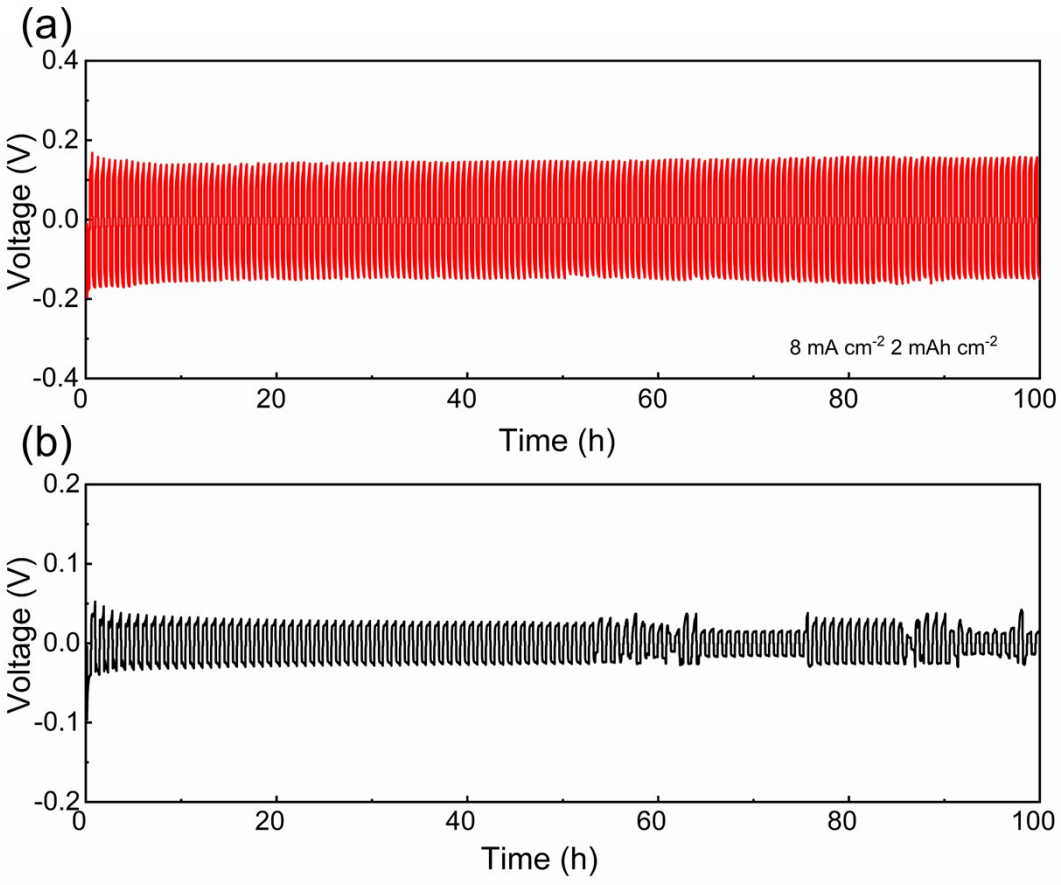

Figure S21. Zn//Zn symmetrical cells with a) Zn@P(SBMA-*co*-BuA) and b) bare Zn at 8 mA cm^{-2} and 2 mAh cm^{-2}.

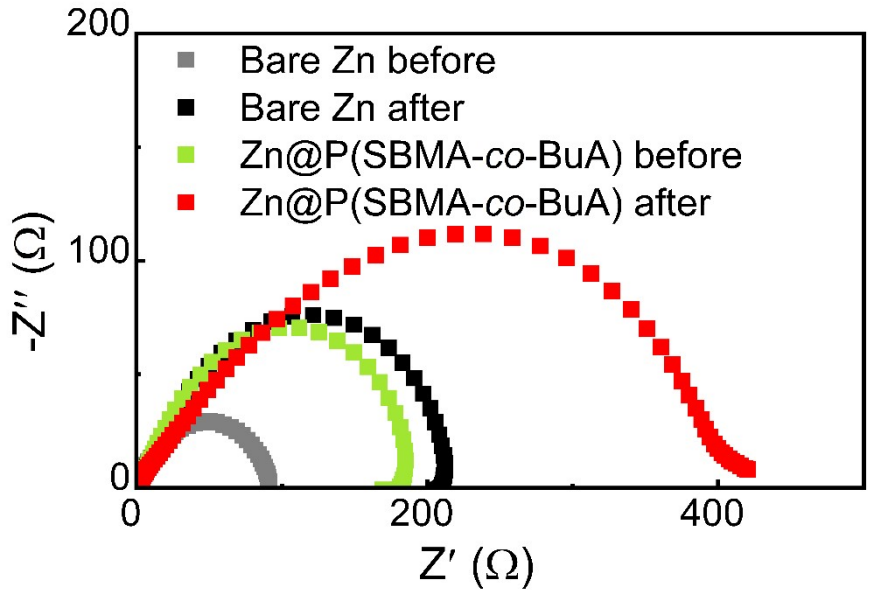

Figure S22. Nyquist plots of symmetric cells using Zn@P(SBMA-*co*-BuA) and bare Zn before cycling and after 50 cycles.

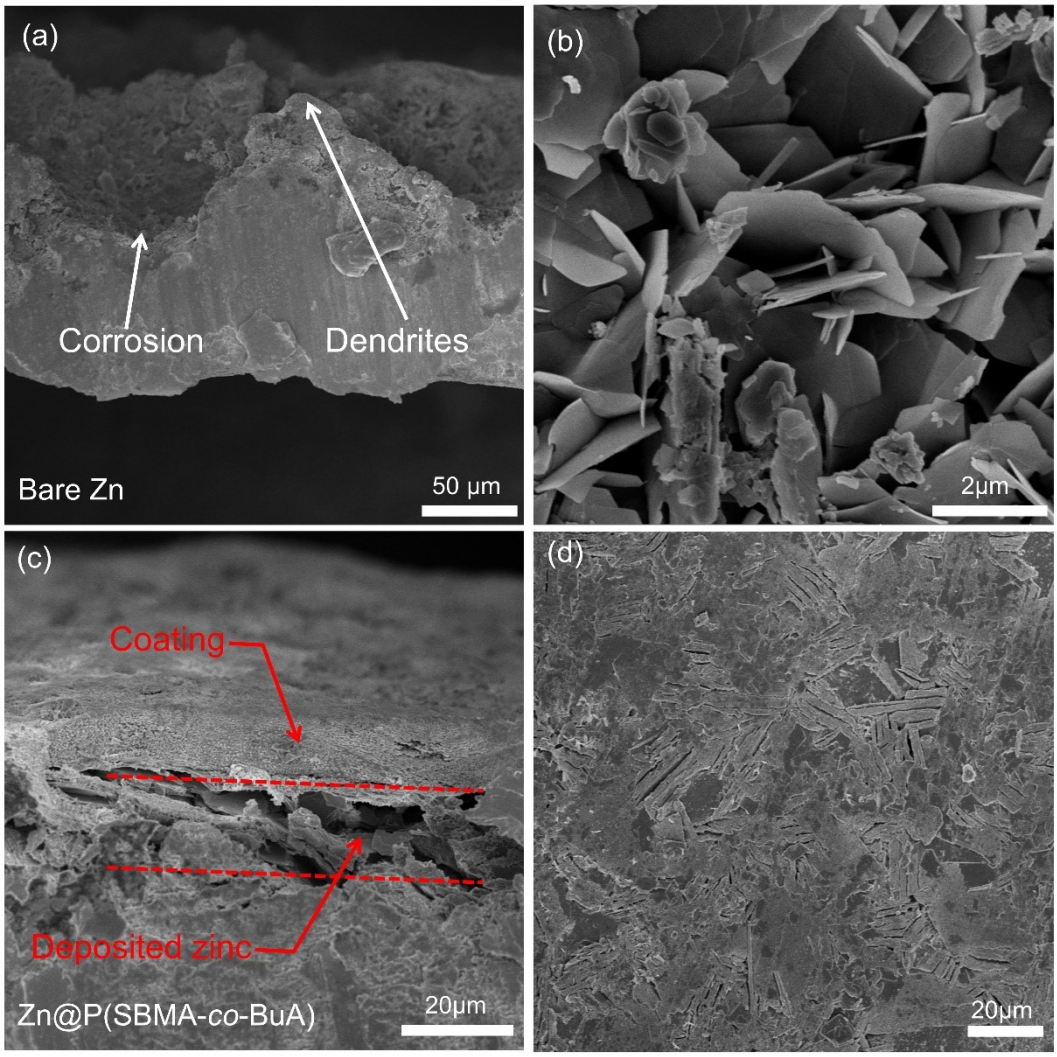

Figure S23. The side-view of a) bare Zn. b) The high magnification image of bare Zn. c) The side-view of Zn@P(SBMA-*co*-BuA) electrode. d) Zn anode image after peeling off the P(SBMA-*co*-BuA) coating.

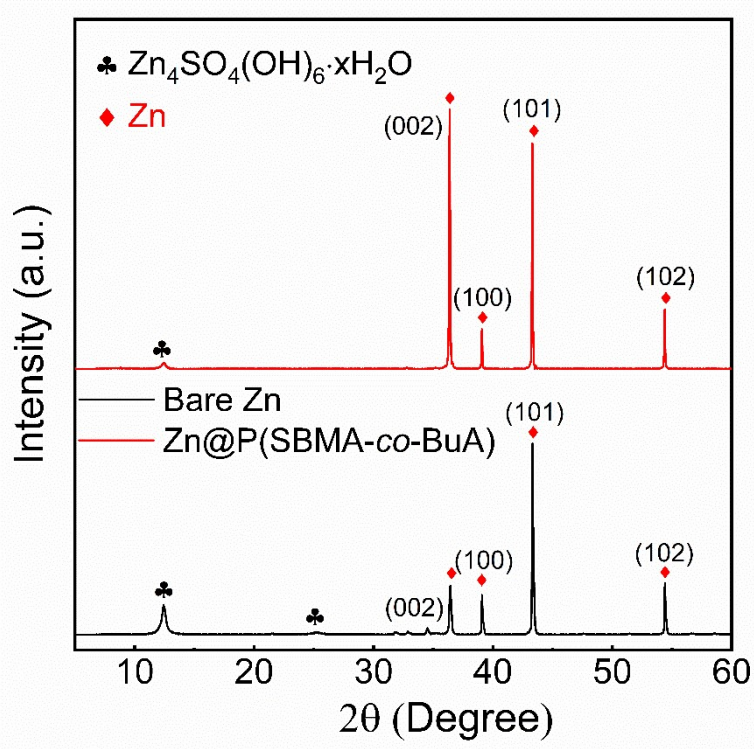

Figure S24. XRD patterns of bare Zn and Zn@P(SBMA-*co*-BuA) electrodes.

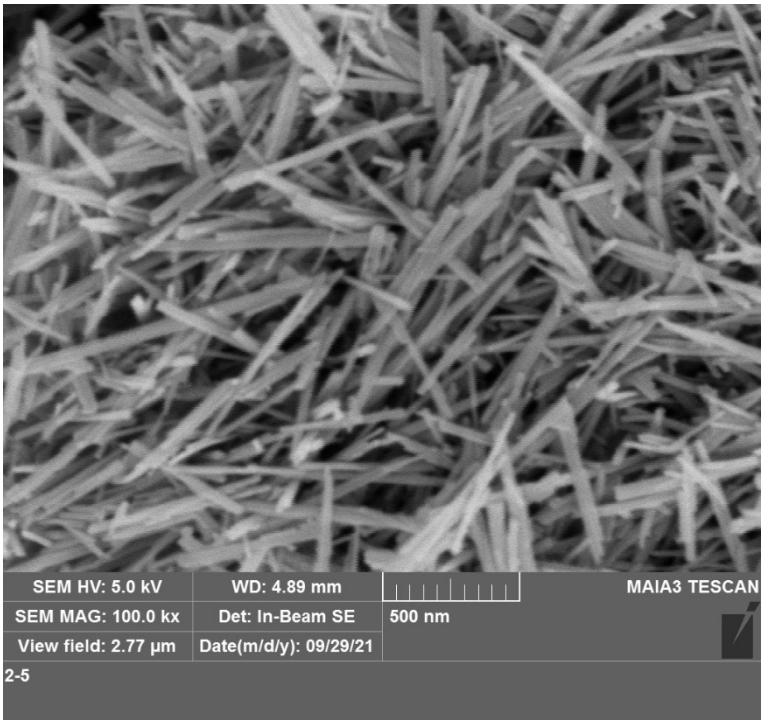

Figure S25. The SEM image of MnO_2 cathode material.

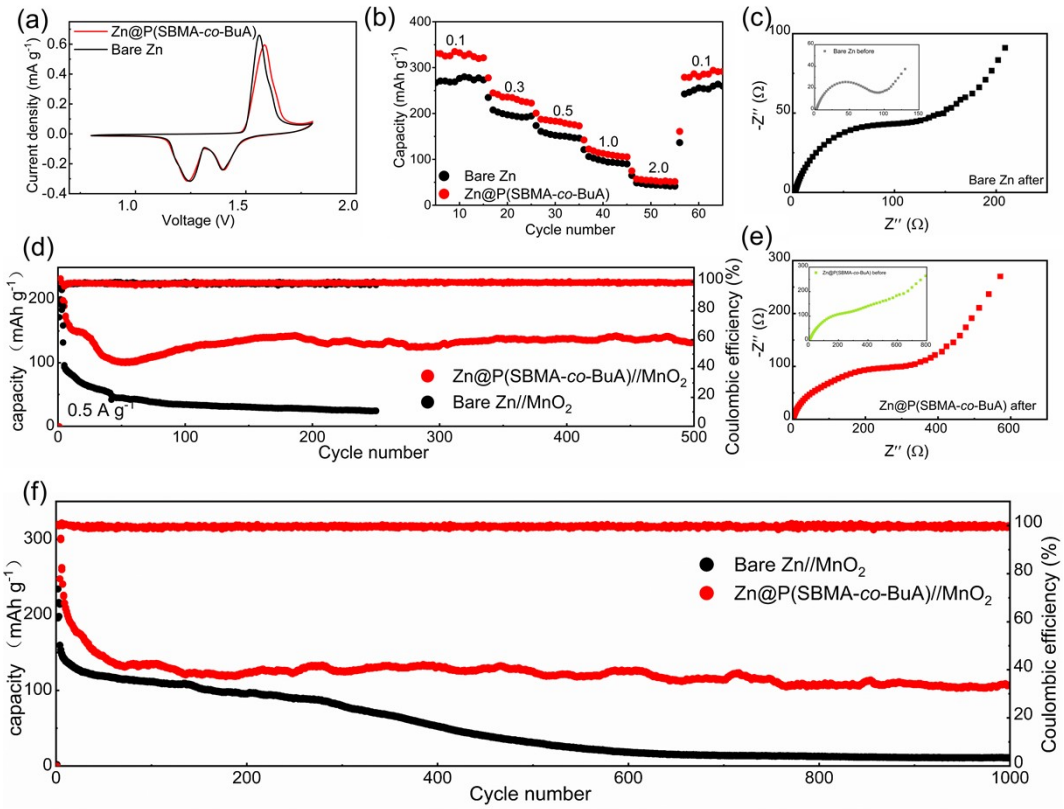

Figure 26. a) CV curves of the Zn//MnO_2 and Zn@P(SBMA-*co*-BuA)//MnO_2 full cell. b) Rate performance. c) Nyquist plots of full cells using bare Zn and (d) Zn@P(SBMA-*co*-BuA) after 100 cycles. e) Cycling performance of the Zn//MnO_2 and Zn@P(SBMA-*co*-BuA)//MnO_2 full cell at the current density of 0.5 A g^{-1} and f) 1A g^{-1}.

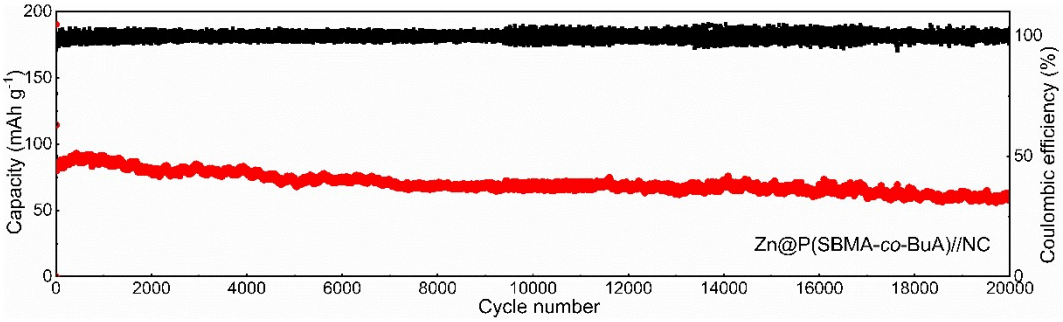

Figure S27. Long-term cycling performance of the Zn@P(SBMA-*co*-BuA)//NC hybrid Zn ion capacitors at the current density of 1 A g^{-1}.

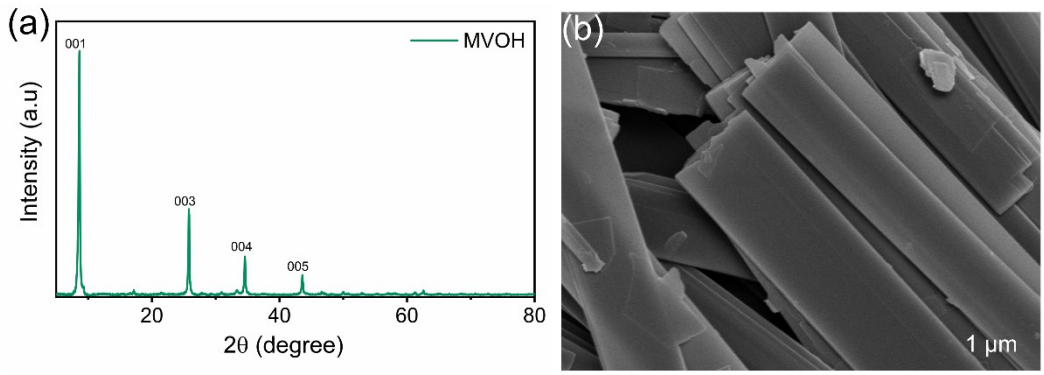

Figure S28. The XRD image and SEM image of MOVH cathode material.

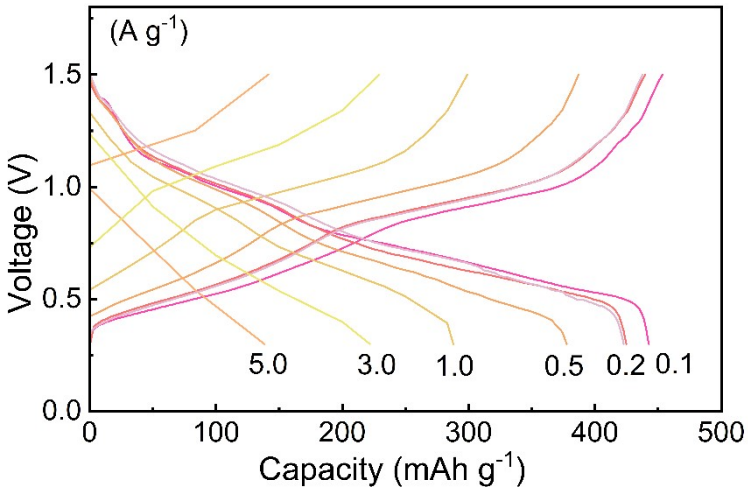

Figure S29. The charge and discharge voltage profiles of full cells with bare Zn anodes.

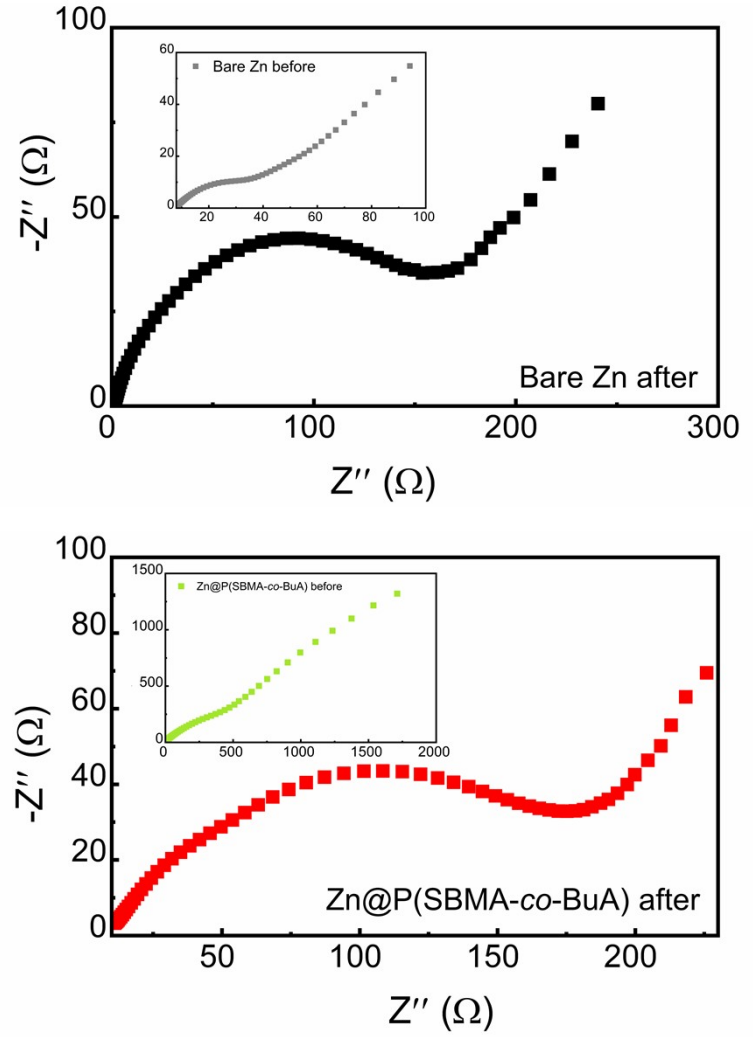

Figure S30. Nyquist plots of full cells using bare Zn and (d) Zn@P(SBMA-*co*-BuA) after 100 cycles.

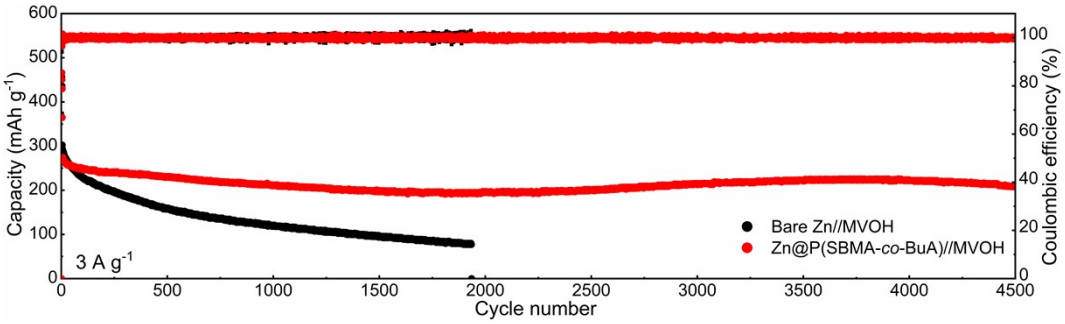

Figure S31. Long cycle performance of the Zn//MVOH and Zn@P(SBMA-*co*-BuA)//MVOH full cell at the current density of 3 A g^{-1}.

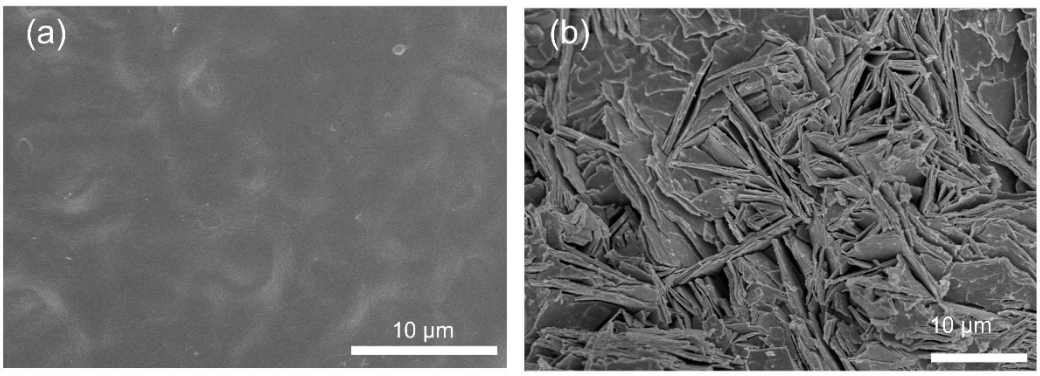

Figure S32. The SEM images of a) Zn@P(SBMA-*co*-BuA) and b) Bare Zn after 100 cycles at 5 A g^{-1}.

.

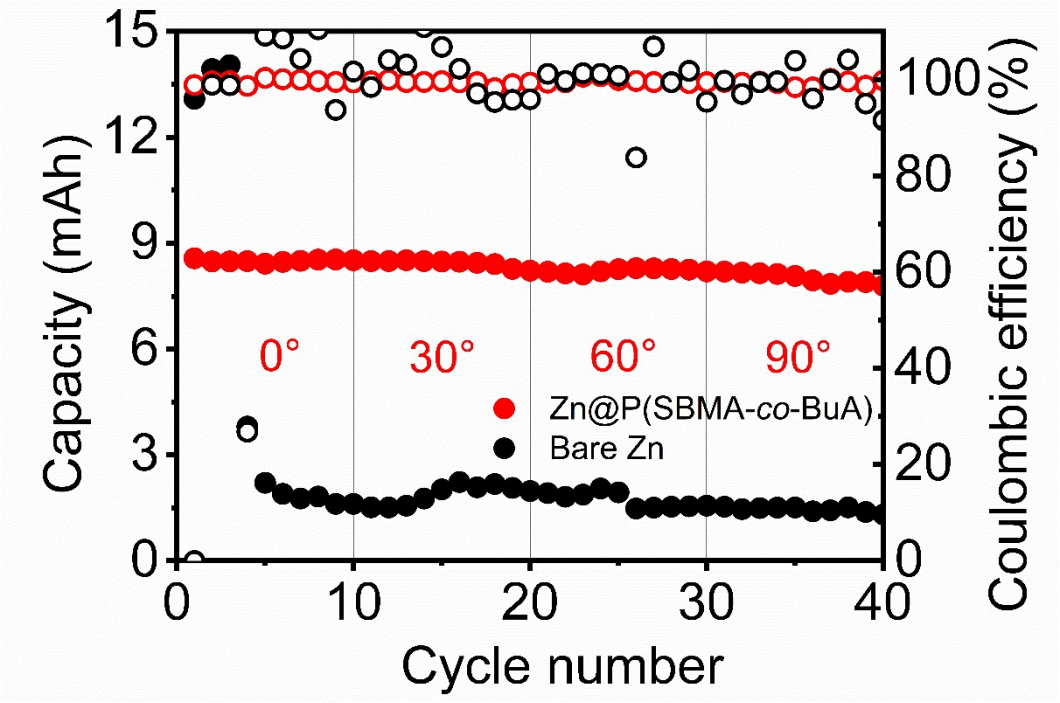

Figure S33. Capacity of a flexible Zn@P(SBMA-*co*-BuA)//MVOH cell tested at 0.5 A g^{-1} under different bending angles.

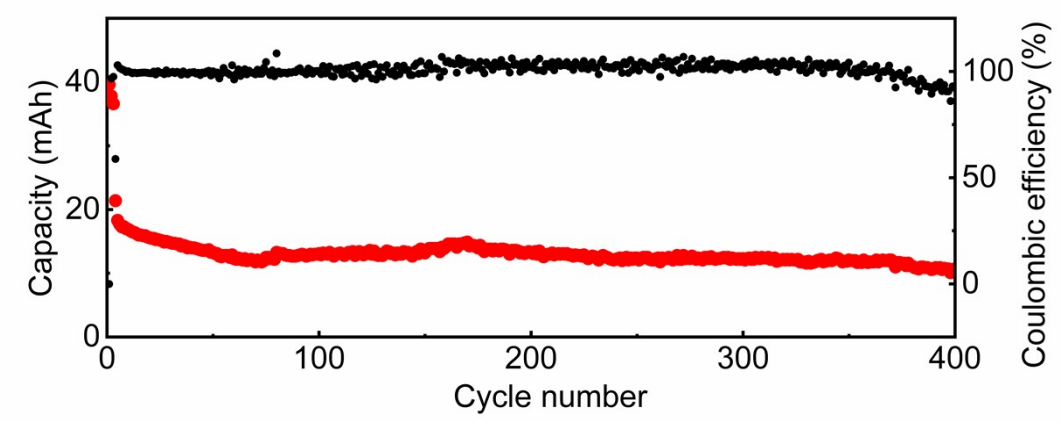

Figure S34. Long cycle performance of Zn@P(SBMA-*co*-BuA)//MVOH pouch cell at 6 A g^{-1}.